Received 15 December 2020; revised 4 February 2021 and 22 March 2021; accepted 12 April 2021. Date of publication 14 April 2021; date of current version 21 April 2021. The review of this article was arranged by Editor M. K. Radhakrishnan.

Digital Object Identifier 10.1109/JEDS.2021.3073220

Direct Defect-Level Analysis of Metal–Insulator–Metal Capacitor Using Internal Photoemission Spectroscopy

TAE JIN YOO [1], HYEON JUN HWANG[1], SOO CHEOL KANG [2], SUNWOO HEO[2], HO-IN LEE[1], YOUNG GON LEE [3], HOKYUNG PARK[3], AND BYOUNG HUN LEE [1] (Senior Member, IEEE)

1 Center for Semiconductor Technology Convergence, Department of Electrical Engineering, Pohang University of Science and Technology, Pohang 37673, South Korea
2 School of Material Science and Engineering, Gwangju Institute of Science and Technology, Gwangju 61005, South Korea
3 Device Modeling & Reliability Group, Research and Development Division, SK Hynix Inc., Icheon 17336, South Korea

CORRESPONDING AUTHOR: B. H. LEE (e-mail: bhlee1@ postech.ac.kr)

This work was supported in part by Creative Materials Discovery Program on Creative Multilevel Research Center under Grant 2015M3D1A1068062 and Grant 2017M3D1A1040828; in part by Nano Materials Technology Development Program under Grant 2016M3A7B4909942; and in part by the Global Frontier Program through the Global Frontier Hybrid Interface Materials (GFHIM) through the National Research Foundation (NRF) of Korea funded by the Ministry of Science and ICT, South Korea, under Grant 2013M3A6B1078873.

ABSTRACT Barrier height (ϕ_b), trap state, bandgap (E_g), and band alignment information of the metal–ZrO_2–metal capacitor have been extracted using internal photoemission (IPE) system. By correlating the IPE analysis with I-V and C-V characteristics obtained before and after rapid thermal annealing, origin and transformation of defect states have been successfully investigated. Our analysis revealed that deep-level defects originating from oxygen vacancies near the top electrode are causing of leakage current in MIM capacitor and these defects can be effectively reduced by a proper thermal annealing.

INDEX TERMS Defect, internal photoemission, metal-insulator-metal (MIM), zirconium oxide.

I. INTRODUCTION

Internal photon-emission (IPE) spectroscopy has been employed to characterize the barrier height, trap states, and bandgap of metal–insulator–metal (MIM) or metal–insulator– semiconductor (MIS) capacitors [1]. IPE is often used to investigate origin of leakage current in MIS or MIM structures [2]–[6]. Cimino *et al.* studied band offset and bandgap of a TiN/HfO_2/TiN capacitor using IPE [3], and Pešić *et al.* examined barrier height between top electrode and ZrO_2/Al_2O_3/ZrO_2 stacked structure [4]. Nguyen *et al.* and Lee *et al.* reported the energy level of defect states at metal/insulator interface of a MIM capacitor by correlating results of spectroscopic ellipsometry and ultraviolet photoelectron spectroscopy (UPS) analysis [2], [6].

IPE provides information for both interfaces and bulk defects using photon-induced excitation. On the other hand, electrical analysis methods, such as capacitance–frequency (C–f) and capacitance–voltage (C–V) measurements, can be used to separate the contributions from interface and bulk defects of the MIM capacitor [7]. Thus, a more systematic analysis of defect states can be performed by combining IPE and AC characterization results.

In this study, we performed I-V, C-V, and IPE characterizations of metal–ZrO_2–metal MIM capacitors before and after rapid thermal annealing (RTA) process to establish correlation between changes in the energy level and density of defects due to the RTA process and the electrical characteristics of ZrO_2 MIM capacitor. Our work provides an example of the novel manner in which IPE analysis and the electrical characterization of MIM capacitors can be combined to reveal changes in the physical properties of a dielectric material, especially its defect states. In addition, the physical changes of MIM capacitor are correlated to the results from IPE and electrical characterization.

II. MEASUREMENT SETUP

The setup diagram of IPE used in this work is shown in Fig. 1(a). Xe lamp (150 W) was used as light source; the light was isolated to specific wavelength after passing through a bandpass filter and monochromatic mirror. The sample unit

was irradiated with this discrete-wavelength light through an optical fiber. A precision semiconductor parameter analyzer (Agilent 4156C) was used to measure the photocurrent and dark current. The quantum yield, representing number of charge carriers generated by the photon, was calculated using the following equation:

$$Y = \frac{I_p h\nu}{PA} = C(h\nu - \phi)^p \tag{1}$$

where I_p represents photocurrent measured by electrical measurement and obtained by subtracting the dark current; $h\nu$ represents the photon energy; P represents the power of light at each wavelength; A is the area of the capacitor; C is the correction constant; ϕ is the barrier height; and p is the polynomial constant, which is having a value of 2 for the metal/dielectric interface.

III. RESULT AND DISCUSSION

In this section, the results of the J–V, C–V, and IPE analysis of the MIM capacitor before and after RTA are analyzed to find a way to correlate the data with each other. Fig. 1(c) shows the leakage current reduction by RTA. The leakage current decreased uniformly in the $+V_g$ region (substrate injection case) with a signature of direct tunneling at the V_g higher than 1.5 V. On the other hand, in the $-V_g$ region (gate injection case), the leakage current drastically decreased, showing very weak direct tunneling even in the high field region (> -1.5 V).

To obtain the insight on the current mechanism, the J-V curves shown in Fig. 2 (a), (b) were fitted using poole-frenkel (P-F) model and trap assisted tunneling (TAT) model which are valid for high and low electric field, respectively [4], [6]. The leakage current following P-F model passes through the barrier between metal and insulator at high electric field. In the case of TAT model the leakage current is generated by hopping mechanism, carriers jumping through the trap sites [4], [6]. Prior to RTA, the P-F current was dominant at high field region (>0.8V) and TAT current was dominant at low field region (<0.8V). After the RTA, the P-F current seems to be reduced, especially for top injection case (V_{app} <0), but the P-F and TAT current was maintained in case of the bottom injection (V_{app} >0). These asymmetric electrical characteristics of the physically symmetric MIM capacitor indicate that there might be a significant change in the band alignment between the electrode materials and ZrO_2 and the distribution of defects in the ZrO_2 layer. We expect that a compositional change in the electrode during the RTA may have occurred asymmetrically, which in turn affected the leakage current mechanism.

Frequency dependence and hysteresis of normalized capacitance (C/C_0) curves were characterized before and after RTA; it shows significant changes, especially in the $-V_g$ region, as shown in Fig. 3 (a) and (b). C–f curves measured at 0 V clearly demonstrate that there was a significant improvement in the dielectric quality, indicating that the defects in ZrO_2 that contributed to the strong dispersion

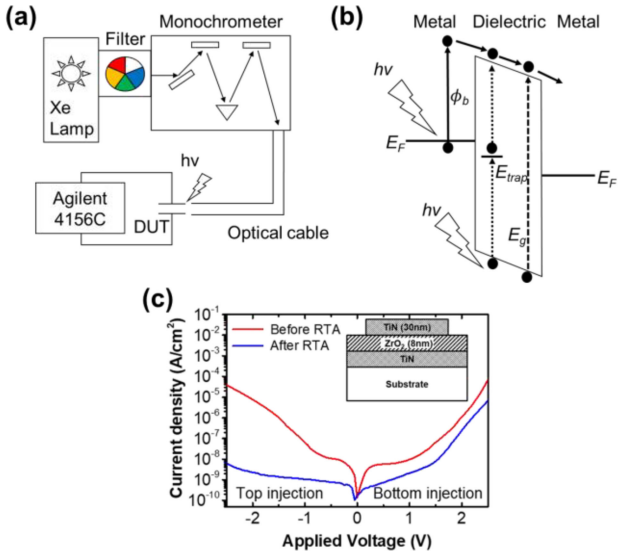

FIGURE 1. Experimental setup of internal photoemission spectroscopy (IPE). (b) Operational principle of IPE method. (c) Current density–applied voltage (J–V) curve measured before and after RTA in N2. Inset figure illustrates the metal-insulator-metal device stack used in this experiment.

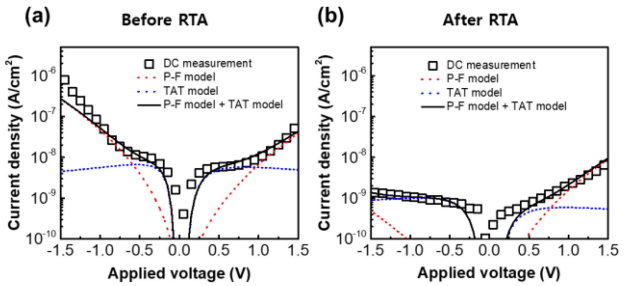

FIGURE 2. J-V characteristics of metal-insulator-metal capacitor. (a) Before RTA and (b) after RTA.

had been reduced after RTA (Fig. 3(c)). Interestingly, the peaks in the C/C_0 curves observed in all frequency regions at ~ -0.7 V before RTA were significantly reduced and moved to $\sim$ 0 V after RTA. Because the C–V measurement reflects the charge exchange between electrode and defect sites, this change implies that the defects responding at -0.7 V were successfully suppressed by RTA. Since the oxygen vacancies are most significantly affected by the RTA, we guess that the peak at -0.7 V might be originated from the oxygen vacancy level. Further, the similar frequency dependence of the hump near (-0.7 V) indicates that the physical locations of trap sites incurring the peak were close to the top electrode [7], [9]. The capacitance density was changed significantly after the RTA, especially at high frequency region. The capacitance density reduction (from 10kHz to 500kHz) was 29% from RTA in N_2 ambience annealed sample and 55% for the unannealed sample. The similar frequency dependence of capacitance was observed from amorphous ZrO_2 film [11].

Further, IPE showed significant changes in the density and energy level of physical defects in ZrO_2. IPE measurements

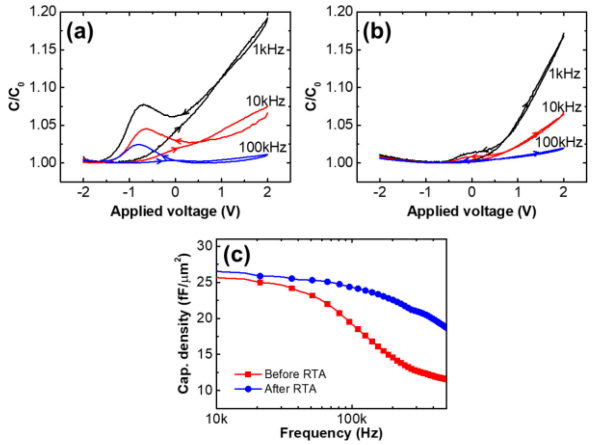

FIGURE 3. **Capacitance–voltage (C–V) and capacitance–frequency (C–f) curves of MIM capacitor; (a) before and (b) after RTA. (c) C–f curve measured at 0 V before and after RTA from 10 kHz to 500 kHz.**

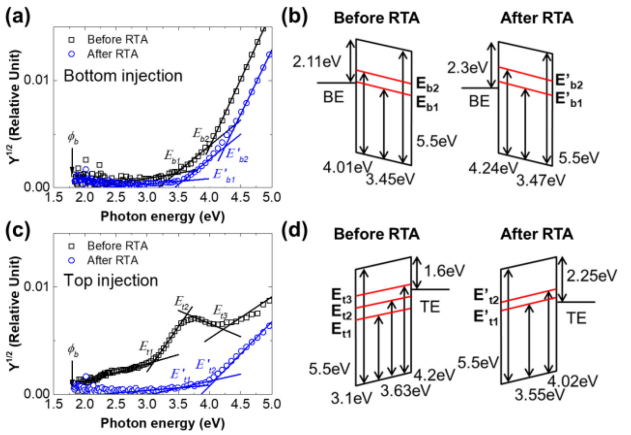

FIGURE 4. **(a), (c) IPE curves measured before and after RTA under applied voltage of 0.6 V for bottom and top injection, respectively. Schematic of the inner band structure of dielectric for (b) bottom and (d) top injection.**

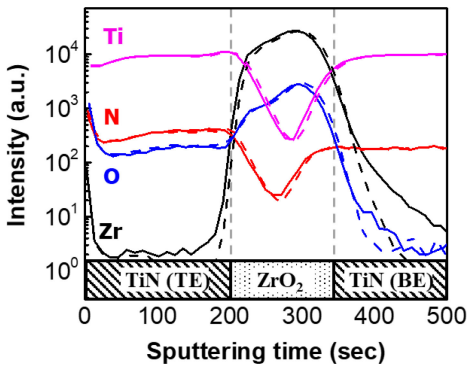

FIGURE 5. **Secondary ion mass spectrometry (SIMS) result of the prepared MIM device before RTA (dotted line) and the after RTA (solid line).**

were conducted at different bias polarities to examine the differences between the top and bottom injection cases. The bandgap of these devices ~ 5.5 eV were not affected by the RTA as previously reported for ZrO_2 films [12], [13]. Several defect levels were observed, as shown in Fig. 4 (a) and (c). The defect levels at 3.0 and 3.5–3.8 eV can be attributed to the oxygen vacancy, while the defect levels at 4.0–4.2 eV are associated with the interstitial defects originated by missing Zr atoms in the ZrO_2 [10], [14].

In the case of the bottom injection, the barrier height increased to 2.3 eV from 2.11 eV after RTA. After the RTA process, the defect level related to interstitial defects increased (E'_{b2}, 4.24 eV), but that of the oxygen vacancy level was constant (E'_{b1}, 3.47 eV). In the case of top injection (negative bias region), the barrier height significantly increased to 2.25 eV from 1.6 eV due to the compositional change after RTA, which explains the drastic leakage current reduction in the $-V_G$ region. The defect level of E_{t2}(3.63 eV) can be attributed to the oxygen vacancy, and E_{t3} (4.2 eV) appears to have originated from the interstitial defect of the zirconium atom. These defect levels are similar to E'_{b1} and E'_{b2} of the bottom injection case. For the case of top injection, an additional defect level related to the oxygen vacancy was observed at E_{t1} (3.1 eV) before RTA [15], but this kind of defect became negligible after RTA.

Finally, secondary ion mass spectroscopy (SIMS) depth profiling was performed to analyze the change in the atomic distribution after the RTA. The depth profiles of Ti, Zr, O and N are shown in Fig. 5. The concentrations of titanium are similar for both top and bottom electrodes, but nitrogen concentration in the top electrode was higher than that of bottom electrode.

Oxygen concentration was relatively high at the top electrode compared to the bottom electrode due to the oxidation of top electrode due to the air exposure. The higher content of oxygen atom near top electrode seems to be due to the oxygen atom substitution to nitrogen atoms in TiN or TiO_xN_y formation after the RTA [15], [16]. In the case of Zr atom, the concentration at the top electrode and bottom electrode are quite different. It appears that the diffusion of Zr might be affected by the oxygen concentration. When oxygen concentration is high, the diffusion of Zr atoms is significantly retarded, which is a reasonable conjecture because the diffusivity of oxidized Zr should be much lower than Zr atoms.

In summary, the large leakage current observed before RTA appears to be originated from the defects having energy levels lower than the Fermi level of metal, especially at 3.1 eV. Thus, the drastic reduction in the leakage current can be attributed to the increase in barrier height and passivation of defects at 3.1 eV. The strong changes in the frequency dependence and yield curves of IPE for the case of top injection indicate that the RTA process primarily affected the oxygen vacancies near the top electrode.

IV. CONCLUSION

The changes in the electrical characteristics and defect states of the MIM capacitor are correlated by comparing the results of the I–V, C–V, SIMS and IPE analysis. In addition to the changes in the Schottky barrier height, we determined that deep-level defects originating from oxygen vacancies near

the top electrode of the MIM capacitor are the origin of the high leakage current. Such leakage current and dispersion could be reduced by RTA treatment. Overall, a strong correlation between the IPE measurement and the electrical characteristics of the MIM capacitor has been established, confirming that the IPE can be used to monitor the electrical characteristics of MIM capacitor.

REFERENCES

[1] V. V. Afanas'ev, *Internal Photoemission Spectroscopy: Fundamentals and Recent Advances*. London, U.K.: Elsevier, 2014.
[2] N. V. Nguyen, O. A. Kirillov, and J. S. Suehle, "Band alignment of metal-oxide-semiconductor structure by internal photoemission spectroscopy and spectroscopic ellipsometry," *Thin Solid Films*, vol. 519, no. 9, pp. 2811–2816, 2011.
[3] S. Cimino *et al.*, "A study of the leakage current in TiN/HfO_2/TiN capacitors," *Microelectron. Eng.*, vol. 95, pp. 71–73, Jul. 2012, doi: 10.1016/j.mee.2011.03.009.
[4] M. Pešić *et al.*, "Conduction barrier offset engineering for DRAM capacitor scaling," *Solid-State Electron.*, vol. 115, pp. 133–139, Jan. 2016, doi: 10.1016/j.sse.2015.08.012.
[5] N. V. Nguyen, O. Kirillov, H. D. Xiong, and J. S. Suehle, "Internal photoemission spectroscopy of metal gate/high-k/semiconductor interfaces," *AIP Conf. Proc.*, vol. 931, no. 1, pp. 308–314, Sep. 2007, doi: 10.1063/1.2799389.
[6] S. Y. Lee *et al.*, "Investigation of ultrathin Pt/ZrO_2–Al_2O_3–ZrO_2/TiN DRAM capacitors Schottky barrier height by internal photoemission spectroscopy," *Current Appl. Phys.*, vol. 17, no. 2, pp. 267–271, Feb. 2017, doi: 10.1016/j.cap.2016.12.004.
[7] S. Hlali, N. Hizem, L. Militaru, A. Kalboussi, and A. Souifi, "Effect of interface traps for ultra-thin high-k gate dielectric based MIS devices on the capacitance-voltage characteristics," *Microelectron. Rel.*, vol. 75, pp. 154–161, Aug. 2017, doi: 10.1016/j.microrel.2017.06.056.
[8] V. V. Afanas'ev and A. Stesmans, "Internal photoemission at interfaces of high-κ insulators with semiconductors and metals," *J. Appl. Phys.*, vol. 102, no. 8, Oct. 2007, Art. no. 081301, doi: 10.1063/1.2799091.
[9] L. Khomenkova, B. S. Sahu, A. Slaoui, and F. Gourbilleau, "Hf-based high-k materials for Si nanocrystal floating gate memories," *Nanoscale Res. Lett.*, vol. 6, no. 1, p. 172, Feb. 2011, doi: 10.1186/1556-276X-6-172.
[10] R. Espinoza-González, E. Mosquera, Í. Moglia, R. Villarroel, and V. M. Fuenzalida, "Hydrothermal growth and characterization of zirconia nanostructures on non-stoichiometric zirconium oxide," *Ceram. Int.*, vol. 40, no. 10, pp. 15577–15584, Dec. 2014, doi: 10.1016/j.ceramint.2014.07.034.
[11] S. Kumar and A. K. Ojha, "Oxygen vacancy induced photoluminescence properties and enhanced photocatalytic activity of ferromagnetic ZrO_2 nanostructures on methylene blue dye under ultra-violet radiation," *J. Alloys Compd.*, vol. 644, pp. 654–662, Sep. 2015, doi: 10.1016/j.jallcom.2015.04.183.
[12] J.-H. Kim, V. A. Ignatova, J. Heitmann, and L. Oberbeck, "Deposition temperature effect on electrical properties and interface of high-kZrO_2 capacitor," *J. Phys. Appl. Phys.*, vol. 41, no. 17, Aug. 2008, Art. no. 172005, doi: 10.1088/0022-3727/41/17/172005.
[13] S. Sayan *et al.*, "Structural, electronic, and dielectric properties of ultrathin zirconia films on silicon," *Appl. Phys. Lett.*, vol. 86, no. 15, Apr. 2005, Art. no. 152902, doi: 10.1063/1.1864235.
[14] M. Varshney, A. Sharma, K. H. Chae, S. Kumar, and S. O. Won, "Electronic structure and dielectric properties of ZrO_2-CeO_2 mixed oxides," *J. Phys. Chem. Solids*, vol. 119, pp. 242–250, Aug. 2018, doi: 10.1016/j.jpcs.2018.04.007.
[15] L. Kumari *et al.*, "Controlled hydrothermal synthesis of zirconium oxide nanostructures and their optical properties," *Crystal Growth Design*, vol. 9, no. 9, pp. 3874–3880, Sep. 2009, doi: 10.1021/cg800711m.
[16] J.-H. Kim, V. Ignatova, P. Kücher, J. Heitmann, L. Oberbeck, and U. Schröder, "Physical and electrical characterization of high-k ZrO_2 metal–insulator–metal capacitor," *Thin Solid Films*, vol. 516, no. 23, pp. 8333–8336, Oct. 2008, doi: 10.1016/j.tsf.2008.03.051.
[17] C. L. Hinkle *et al.*, "Interfacial oxygen and nitrogen induced dipole formation and vacancy passivation for increased effective work functions in TiN/HfO_2 gate stacks," *Appl. Phys. Lett.*, vol. 96, no. 10, Mar. 2010, Art. no. 103502, doi: 10.1063/1.3353993.

TAE JIN YOO received the Ph.D. degree in materials science and engineering from the Gwangju Institute of Science and Technology, Gwangju, South Korea. His research interests include graphene and 2-D material-based optoelectronic device technology.

HYEON JUN HWANG received the Ph.D. degree in materials science and engineering from the Gwangju Institute of Science and Technology, Gwangju, South Korea. His current research interests are extreme low-power electronic device with ferroelectric HZO and FeFET memory device with graphene and 2-D materials.

SOO CHEOL KANG received the Ph.D. degree in material science and engineering from the Gwangju Institute of Science and Technology, Gwangju, South Korea. His current research interests include emerging device reliability.

SUNWOO HEO received the Ph.D. degree in materials science and engineering from the Gwangju Institute of Science and Technology, Gwangju, South Korea. His current research interests include emerging device technologies, device reliability, and process integration for memory technologies.

HO-IN LEE is currently pursuing the Ph.D. degree in electrical engineering with the Pohang University of Science and Technology, Pohang, South Korea. His research interests are focused on the electrical characterization, compact model design, and performance evaluation of low power electronics.

YOUNG GON LEE received the Ph.D. degree in materials science and engineering from the Gwangju Institute of Science and Technology, Gwangju, Korea, in 2015. He has been a Senior Engineer with SK Hynix, since 2015. His current research interests include device characterization and reliability physics of semiconductor device.

HOKYUNG PARK received the Ph.D. degree in materials science and engineering from the Gwangju Institute of Science and Technology, Gwangju, Korea, in 2007. He has been a Project Leader of Device Reliability with Research and Development Division, SK Hynix, since 2016. His current research interests include device characterization and reliability physics of logic/memory device.

BYOUNG HUN LEE (Senior Member, IEEE) received the Ph.D. degree in electrical and computer engineering from the University of Texas at Austin, Austin, TX, USA, in 2000. His current research interests include extreme low-power electronic and photonic device technology using graphene and 2-D materials and the development of electrical characterization methods for silicon devices.